The compound-choking theory as an explanation of the entrainment limitation in supersonic ejectors

Olivier Lamberts[a,*], Philippe Chatelain[a], Nicolas Bourgeois[a], Yann Bartosiewicz[a]

[a] *Institute of Mechanics, Materials and Civil Engineering (iMMC), Université catholique de Louvain (UCL), Louvain-la-Neuve, 1348, Belgium*

Abstract

While the limitation of the entrainment ratio in supersonic ejectors is a well-known phenomenon, there is still a need to gain insight on the choking phenomena at play in on-design operation. In state-of-the-art simplified models of supersonic ejectors, the secondary stream is assumed to reach sonic velocity in a hypothetical throat (Fabri-choking). However, an alternative explanation of the entrainment limitation known as the compound-choking theory states that a nozzle flow with two streams at different stagnation pressures may be choked with a subsonic stream if the other one is supersonic. In this paper, the compound-choking is highlighted in a supersonic ejector through a thorough analysis of numerical simulations validated against experimental data. In addition, comprehensive experimental data of supersonic ejectors are used to assess the performance of the compound-choking theory to predict the entrainment ratio in the on-design regime in various configurations. Most predictions are in the $\pm 10\%$ range when compared to the experimental data. Compared to state-of-the-art 1D models relying on the Fabri-choking assumption, the compound-choking theory is shown to generally perform better regarding the prediction of the on-design entrainment ratio. This study suggests that the compound-choking theory is well suited to model the choking process in supersonic ejectors.

Keywords: Supersonic ejector, Compound-choking, Fabri-choking, CFD

---

*Corresponding author

Email address: `olivier.lamberts@uclouvain.be` (Olivier Lamberts)

NOMENCLATURE

A	Cross-sectional area [m^2]
A_m	Cross-sectional area of the mixing duct [m^2]
A_t	Cross-sectional area of the throat of the primary nozzle [m^2]
ER	Entrainment ratio [-]
H_1	Height of the exit of the primary nozzle [m]
H_m	Height of the mixing duct [m]
H_t	Height of the throat of the primary nozzle [m]
M	Mach number [-]
M_{eq}	Equivalent Mach number [-]
$\dot{m}$	Mass flow rate [kg/s]
p	Static pressure [bar]
p^*	Static pressure at sonic conditions [bar]
p^*_{eq}	Static pressure at compound-sonic conditions [bar]
R	Specific gas constant [J/K/kg]
T	Static temperature [K]
$\mathbf{u}$	Velocity vector field [m/s]
x	Horizontal coordinate [m]
y	Vertical coordinate [m]
z	Span-wise coordinate [m]

Special characters

β	Compound-flow indicator [m^2]
γ	Specific heat ratio [-]
μ	Dynamic viscosity [Ns/m^2]
ρ	Density [kg/m^3]
ω	Specific turbulence dissipation rate [1/s]

Subscripts

ref	Reference conditions
0	Reservoir conditions
1	Value associated to the primary stream
2	Value associated to the secondary stream

1. Introduction

The fundamental role of a supersonic ejector consists in the compression of a secondary (or entrained) fluid stream at a low stagnation pressure through exergy exchanges with a primary (or motive) stream at a higher stagnation pressure. One of the main advantages of the ejector lies in its geometrical simplicity (and the resulting reliability), as it simply consists in a primary nozzle whose exit section is placed at the entry of a secondary nozzle (see Fig. 1). In general, the external nozzle has an elongated throat called the mixing duct (or mixing chamber), and the exit of the primary nozzle lies in the converging part of the secondary nozzle.

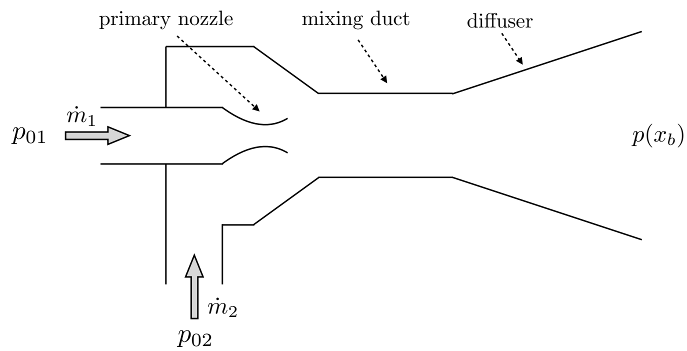

Figure 1: Typical layout of a supersonic ejector.

As reported in Zegenhagen and Ziegler (2015), the geometrical simplicity of a supersonic ejector contrasts with the complex flow phenomena occurring within it, such as choking, turbulent mixing and shock-wave boundary layer interactions to name but a few (Fabri and Siestrunck (1958), Sriveerakul et al. (2007b), Rao and Jagadeesh (2014), Lamberts et al. (2018)). Among all of these flow features, the choking of the flow is of primary importance as it limits the performance of the supersonic ejector (Chou et al. (2001)). Indeed, for fixed reservoir conditions, the entrainment ratio, defined as $\mathrm{ER} = \dot{m}_2/\dot{m}_1$, reaches a plateau once the back-pressure, $p(x_b)$ in Fig. 1, falls below a critical value. Below this critical back-pressure, the flow is choked within the ejector and the latter is said to operate in on-design (or critical) conditions. The term 'double-choking' may also be found in the literature to designate this mode of operation (Zegenhagen and Ziegler (2015), Croquer et al. (2016c)).

While in rare instances the secondary stream is assumed to choke geometrically (Galanis and Sorin (2016), Ameur et al. (2016)), the generally accepted theory for the choking process in supersonic ejectors is based on the early contribution of Fabri and Siestrunck (1958) (Chunnanond and Aphornratana (2004a), Besagni et al. (2016)). Based on wall pressure measurements and flow visualizations in a rectangular ejector, they postulated that the secondary stream reaches sonic velocities a certain distance downstream of the exit of the primary nozzle, in a sort of aerodynamic throat caused by the pinching of the secondary stream between the primary jet and the ejector wall (Fabri and Siestrunck (1958)). In the literature, this sonic section in the secondary stream is also termed the *critical section* (del Valle et al. (2012)), the *effective area* (Munday and Bagster (1977), Chunnanond and Aphornratana (2004b), Chou et al. (2001)) or the *hypothetical throat* (Huang et al. (1999), He et al. (2009), Kong and Kim (2015)). Even though Fabri and Siestrunck (1958) identified this phenomenology of choking as the *supersonic flow pattern*, it is simply designated by the term *Fabri-choking* in the present document, in accordance with other works in the literature (Addy et al. (1981), Lear et al. (2000), Lamberts et al. (2018)).

At about the same time as Fabri and Siestrunck (1958), another theory emerged in the propulsion field for the explanation of the entrainment limitation in supersonic ejectors. Based on a wave velocity argument, Pearson et al. (1958) derived a choked flow condition in the case of two perfect gases with different stagnation pressures flowing through a cylindrical ejector. The obtained condition is such that the flow with the greater total pressure is supersonic while the other is subsonic. An equivalent result has been subsequently reported in Hoge and Segars (1965). In both studies, the measurement of the static pressure at the wall is used to corroborate the fact that the secondary stream remains subsonic as the pressure drop that it experiences is not sufficient for the gas to reach sonic velocities. A few years later, based on the same assumptions as Pearson et al. (1958), Bernstein et al. (1967) developed what they called a one-dimensional compound-compressible nozzle flow theory for analyzing the behavior of one or more gas streams flowing through a single nozzle. The general conclusions of Bernstein et al. (1967) were consistent with the results of Pearson et al. (1958). Note that Bernstein et al. (1967) introduced the term *compound-choking* which is adopted in this study to designate the choking theory presented in their work.

Even though references to the works of Pearson et al. (1958) or Bernstein et al. (1967) are reported in some articles of the following decade related to ejectors (Hedges and Hill (1974), Kurtz (1976)), the authors of the present article hardly found recent studies referring to the compound-choking theory. Indeed, for an unknown reason, the Fabri-choking model is used as the foundation of almost all state-of-the-art simplified models of supersonic ejectors (Huang et al. (1999), Zhu et al. (2007), del Valle et al. (2012), Chen et al. (2013), Zegenhagen and Ziegler (2015), Ma et al.

(2017), Chen et al. (2017)). An in-depth analysis of these models shows that they still have difficulty in predicting the entrainment ratio for on-design operating conditions. Even when real gas effects are taken into account, the average deviation is close to 8% in Zegenhagen and Ziegler (2015), even by using a fitting coefficient, whereas del Valle et al. (2012), who used a perturbation procedure to model 2D features, reported a maximum error of 17%. The same observation can be made in Chen et al. (2017). Hence, despite the considerable effort put over the last decades to model and analyze the flow in supersonic ejectors, there is still a lack of understanding of the choking process in such devices (He et al. (2009), Ruangtrakoon et al. (2013), Mazzelli et al. (2015), Besagni et al. (2016)). This difficulty partially explains why there is no generally accepted methodology for the design of ejectors (Galanis and Sorin (2016)).

The current limitations of 1D models and the development of computational power has lead many research groups to use Computational Fluid Dynamics (CFD) to predict the ejector performance under varying operating conditions and/or geometries (Sriveerakul et al. (2007a), Hemidi et al. (2009a), Varga et al. (2009)). Although the analysis of the numerical results at the local scale could serve the improvement of simplified models, these two approaches have barely been compared (Croquer et al. (2016c), Lamberts et al. (2018)). More interestingly, when focusing on the choking phenomenology, the Fabri-choking has been observed in one study only (Lamberts et al. (2018)). Indeed, in many works where the iso-contour of Mach number unity is shown for on-design operating conditions, the latter is found to progressively expand from the exit of the primary nozzle towards the wall, with no apparent 'sonic section' in the core of the secondary stream (Hemidi et al. (2009b), Ji et al. (2010), Ruangtrakoon et al. (2013), Mazzelli and Milazzo (2015), Croquer et al. (2016b), Croquer et al. (2016c)). Hence, based on numerous numerical simulations of the flow in supersonic ejectors, it appears that the choking process does not necessarily corresponds to the Fabri-choking phenomenology. This issue has never been addressed in the literature.

In the present work, it is shown that the compound-choking theory of Bernstein et al. (1967) yields an explanation for both the absence of a sonic section in most numerical results and the difficulties of state-of-the-art 1D models to predict the on-design entrainment ratio. First, the flow within a rectangular supersonic ejector is simulated through a well validated CFD model (Lamberts et al. (2018)). The numerical results are thoroughly post-processed in order to highlight the choking process at play in on-design operation. For the present ejector geometry and operating conditions, the secondary stream remains subsonic for some on-design operating conditions and the choking phenomenology is properly described by the compound-choking theory. Secondly, based on the experimental data of Huang et al. (1999) which often serve as a benchmark for simplified models, the compound-choking theory in its simplest form is shown to generally perform better than more sophisticated 1D models regarding the prediction of the entrainment ratio in on-design conditions.

This article is structured as follows: the fundamentals of the compound-choking theory are briefly exposed in Section 2, as well as the description of the numerical setup including its experimental validation. Section 3 is split into two parts: the post-processing of the numerical results for the investigation of the choking process for fixed reservoir conditions is proposed in Section 3.1, whereas Section 3.2 is dedicated to the application of the compound-choking theory to predict the on-design entrainment ratio of published experimental ejector configurations, as well as a comparison with state-of-the-art 1D models. The main conclusions and perspectives of the present investigation are summarized at the end of the paper.

2. Material and methods

2.1. Compound-choking theory

2.1.1. Assumptions

The compound-choking theory has been derived in Bernstein et al. (1967) from the concept of a one-dimensional compound-compressible nozzle flow, illustrated in Fig. 2. This theory is based on the following assumptions:

1. the flow in each stream is one-dimensional, steady and isentropic;
2. the static pressure can vary only along the nozzle, implying that it cannot change from stream-to-stream across the nozzle;
3. each fluid is a perfect gas with constant thermodynamic properties.

Note that mixing and real gas effects are thus ignored in the compound-choking theory of Bernstein et al. (1967). Although less explicitly stated, the pioneering contribution of Pearson et al. (1958) essentially relied on the aforementioned assumptions. In what follows, in addition to these assumptions, all the streams are assumed to have identical thermodynamic properties, namely equal specific heat ratios and specific gas constants, noted γ and R, respectively. As a consequence, in the present study, the streams differ from each other only with regard to their reservoir conditions. The general case of perfect gases with different thermodynamic properties is presented in Bernstein et al. (1967).

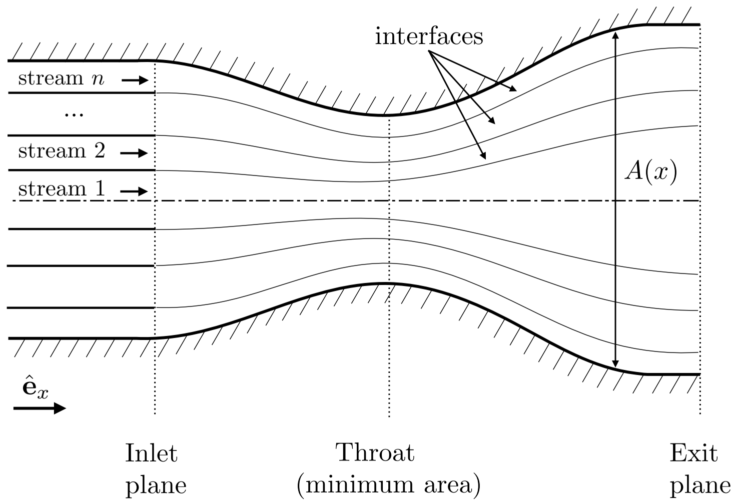

Figure 2: Schematic drawing of the compound-compressible nozzle flow (adapted from Bernstein et al. (1967)).

2.1.2. Compound-choking condition

By deriving the velocity of a so-called compound wave, Bernstein et al. (1967) arrived at the conclusion that the *compound-flow indicator*, $\beta(x)$, defined as

$$\beta(x) = \sum_{i=1}^{n} \frac{A_i(x)}{\gamma} \left(\frac{1}{M_i^2(x)} - 1 \right) \quad , \tag{1}$$

is the key indicator to determine the *compound-flow regime*, i.e. the nature of the flow. In Eq. (1), $A_i(x)$ and $M_i(x)$ represent the local flow area and the local Mach number of the ith stream, respectively. More precisely, it is shown in Bernstein et al. (1967) that the velocity in the upstream direction of a compound wave must always have the same sign as the compound flow indicator, β. Hence, $\beta > 0$, $\beta = 0$ and $\beta < 0$ corresponds to the so-called *compound-subsonic*, *compound-sonic* and *compound-supersonic* regime, respectively. Actually, the compound-choking theory of Bernstein et al. (1967) considers an aerodynamic-based choking just as Fabri and Siestrunck (1958), but based on another criterion for the blockage of the pressure waves. While the focus is put on the secondary stream only in the Fabri-choking theory, the compound-choking theory takes both streams under consideration to analyse the choking process, as the combination of the two streams may behave like a sonic stream (Hoge and Segars (1965)).

In addition, Bernstein et al. (1967) also demonstrated that the compound-choking of the flow can only occur at the nozzle minimum area, i.e. at the location where $A(x)$ is minimum and equal to A_{throat}, for it is there only that β can equal zero. The interested reader is referred to the original publication for more details in deriving these results.

A closer inspection of Eq. (1) leads to the conclusion that, when a compound flow is choked ($\beta = 0$), the individual stream Mach numbers at the throat will not necessarily be equal to one (Bernstein et al. (1967)). More importantly, for flows involving two streams at different stagnation pressures, one stream must be supersonic, yielding $1/M_i^2 < 1$ in Eq. (1), while the other must be subsonic, i.e. $1/M_i^2 > 1$, to have $\beta = 0$. As the static pressure is assumed to be the same in both streams, the supersonic stream will correspond to the fluid with the greater total pressure.

As proposed in Hedges and Hill (1974), when all the streams have the same thermodynamic properties, it is convenient to define an equivalent Mach number, $M_{eq}(x)$, such that

$$M_{eq}(x) = \left(\gamma \frac{\beta(x)}{A(x)} + 1\right)^{-1/2} \quad , \tag{2}$$

where A is the local total flow area (see Fig. 2). This equivalent Mach number offers the advantage of being analogous with the Mach number in single-stream flows with regard to its interpretation. Indeed, M_{eq} will be unity for compound-sonic flow ($\beta = 0$), less than unity for compound-subsonic flow ($\beta > 0$) and greater than unity for compound-supersonic flow ($\beta < 0$) (Hedges and Hill (1974)).

2.1.3. Computational procedure for two-stream compound-compressible nozzle flows

Another achievement of the work of Bernstein et al. (1967) consists in proposing a computational procedure in the case of two-stream convergent-divergent nozzles. First, under the assumptions reported in Section 2.1.1, the mass flow rate of the ith stream may be written as a function of the local pressure $p(x)$ and the local flow area $A_i(x)$ only

$$\dot{m}_i = \frac{A_i(x) p_{0i}}{\sqrt{T_{0i}}} \left(\frac{p(x)}{p_{0i}}\right)^{\frac{1}{\gamma}} \sqrt{\frac{2}{R}\left(\frac{\gamma}{\gamma-1}\right)\left[1 - \left(\frac{p(x)}{p_{0i}}\right)^{\frac{\gamma-1}{\gamma}}\right]} \quad (i = 1,\, 2). \tag{3}$$

The derivation of this equality may be found in classical textbooks like Shapiro (1953) or Zucker and Biblarz (2002). Hence, the geometrical compatibility condition, i.e.

$A_1(x) + A_2(x) = A(x)$, may be written at any point in the nozzle as[1]

$$\frac{\dot{m}_2}{\dot{m}_1}\sqrt{\frac{T_{02}}{T_{01}}} = \left\{ \frac{A(x)}{A_1^*} \left[\left(\frac{2}{\gamma-1}\right) \left(\frac{\gamma+1}{2}\right)^{\frac{\gamma+1}{\gamma-1}} \right]^{1/2} - \left(\frac{p_{01}}{p(x)}\right)^{1/\gamma} \left[1 - \left(\frac{p(x)}{p_{01}}\right)^{\frac{\gamma-1}{\gamma}} \right]^{-1/2} \right\} \times \left[1 - \left(\frac{p(x)}{p_{02}}\right)^{\frac{\gamma-1}{\gamma}} \right]^{1/2} \left(\frac{p_{02}}{p_{01}}\right) \left(\frac{p(x)}{p_{02}}\right)^{1/\gamma} , \tag{4}$$

where

$$A_1^* = \frac{\dot{m}_1 \sqrt{T_{01}}}{p_{01}} \sqrt{\frac{R}{\gamma} \left(\frac{\gamma+1}{2}\right)^{\frac{\gamma+1}{\gamma-1}}} . \tag{5}$$

Under choked flow conditions, a second equation arises from the fact that β, defined in Eq. (1), must fall to zero at the nozzle geometric throat (compound-sonic condition). By using the relation between the Mach number and the ratio of total to static pressures of the ith stream for an isentropic flow, i.e.

$$M_i(x)^2 = \frac{2}{\gamma-1} \left[\left(\frac{p_{0i}}{p(x)}\right)^{\frac{\gamma-1}{\gamma}} - 1 \right] \qquad (i = 1,\, 2), \tag{6}$$

the condition $\beta = 0$ may be rewritten as

$$\frac{\dot{m}_2}{\dot{m}_1}\sqrt{\frac{T_{02}}{T_{01}}} = \left(\frac{p_{02}}{p_{01}}\right)^{\frac{\gamma-1}{\gamma}} \frac{\left\{ \frac{\gamma-1}{2} \left[\left(\frac{p_{eq}^*}{p_{01}}\right)^{\frac{1-\gamma}{\gamma}} - 1 \right]^{-1} - 1 \right\} \left[1 - \left(\frac{p_{eq}^*}{p_{02}}\right)^{\frac{\gamma-1}{\gamma}} \right]^{1/2}}{\left\{ 1 - \frac{\gamma-1}{2} \left[\left(\frac{p_{eq}^*}{p_{02}}\right)^{\frac{1-\gamma}{\gamma}} - 1 \right]^{-1} \right\} \left[1 - \left(\frac{p_{eq}^*}{p_{01}}\right)^{\frac{\gamma-1}{\gamma}} \right]^{1/2}} , \tag{7}$$

where p_{eq}^* represents the static pressure corresponding to the compound-sonic regime ($\beta = 0$). The following dimensionless ratios $\dot{m}_2\sqrt{T_{02}}/\dot{m}_1\sqrt{T_{01}}$, p_{02}/p_{01}, A_{throat}/A_1^* and p_{eq}^*/p_{02} are thus the fundamental dimensionless quantities in the compound-choking theory. As explained in Bernstein et al. (1967), if two of these ratios are known, solving Eqs. 4 and 7 will provide the value of the two others under choked flow conditions, for any value of γ.

[1] Please note that the minus sign in the '-1/2' exponent of the first line in Eq. (4) is missing in the original paper of Bernstein et al. (1967), which is probably a mere oversight.

2.1.4. *Prediction of the entrainment ratio in supersonic ejectors with the compound-choking theory*

By identifying the flow in supersonic ejectors as a two-stream compound compressible nozzle flow, the computational procedure described above may be used to predict the on-design entrainment ratio for known reservoir conditions and a given geometrical configuration. Indeed, if the flow is assumed to be isentropic in the primary nozzle, A_1^* will be equal to the area of the throat of the primary nozzle, A_t. In addition, the cross-section of the mixing duct of a supersonic ejector, A_m, may be identified as the geometrical throat of the compound-compressible nozzle flow considered in Bernstein et al. (1967). Hence, for specified A_m/A_t, p_{02}/p_{01}, T_{02}/T_{01} and γ, the simultaneous resolution of Eqs. 4 and 7 provides a certain entrainment ratio for choked conditions according to the compound-choking theory. The value of p_{eq}^*/p_{02} is the second output of the procedure.

2.2. *Numerical method*

The numerical method of the present CFD calculations has been thoroughly documented in Lamberts et al. (2017). For the sake of brevity, only the principal features of the numerical modelling are presented below.

2.2.1. *Flow solver*

The numerical simulations shown here have been performed with OpenFOAM, which is an open-source software for CFD (Weller et al. (1998)). It uses a Finite Volume method and may be applied both on structured or unstructured grids. The numerical results have been obtained with an unsteady density-based compressible flow solver relying on central-upwind schemes of Kurganov et al. (2001), described in details in Greenshields et al. (2010) and named *rhoCentralFoam*. It solves the compressible Reynolds-Averaged Navier-Stokes (RANS) equations with common approximations (Lamberts et al. (2017)).

For the present numerical results, the effects of turbulence are accounted for using the wall-resolved k-ω-SST turbulence model with a turbulent Prandtl number, Pr_t, set to 0.9 (Wilcox (2006)). This model has been found to yield the best agreement with the experimental measurements concerning both global and local flow quantities in many studies (Bartosiewicz et al. (2003), del Valle et al. (2015), Mazzelli et al. (2015), Croquer et al. (2016a), Besagni and Inzoli (2017)).

As mentioned above, the solver serving for the CFD calculations is not a steady-state solver. In the present study, the criterion that is used to assess the convergence of each simulation is the relative difference between the mass flow rates at the inlet and at the outlet of the computational domain. Once the latter is stabilized between

± 0.05%, the solver is assumed to have reached the steady-state solution. The value of the CFL number is set to 0.5 for all operating conditions. Finally, the working fluid is assumed to be a perfect gas with $R = 287.058$ [J/(kg.K)] and $\gamma = 1.4$.

2.2.2. Ejector geometry

The ejector used in the present work has a rectangular cross section to avoid optical distortion with front and back surfaces made of Plexiglas windows. The primary nozzle has a converging-diverging geometry (see Fig. 3). At the throat of the primary nozzle, the aspect ratio of the cross-section is close to 8, whereas the nozzle exit is characterized by an aspect ratio slightly higher than 6. The aspect ratio of the cross-section of the mixing duct is approximately equal to 1.8 and diminishes towards the exit of the diffuser where it is close to 0.4. The mixing duct is 280.6 [mm] long and the aperture angle of the diffuser is 8 degrees.

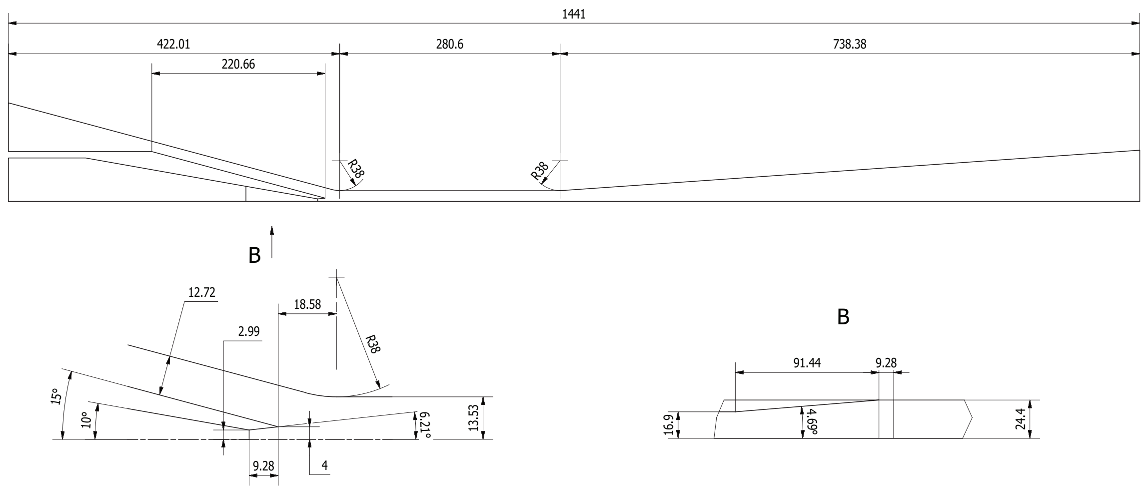

Figure 3: Dimensioned drawing of the ejector used for the experimental investigations and modeled in the numerical simulations. Only one quarter of the entire geometry is shown. All dimensions are in mm.

2.2.3. Computational domain

The rectangular ejector is modelled as a two-dimensional geometry. Due to the relatively small aspect ratio of the diffuser, 3D effects may be important in the off-design regime, but the errors for the prediction of the entrainment ratio are comparable for on-design operating conditions (Mazzelli et al. (2015)). As the focus of this study is put on the choking phenomenology, the analysis is logically restricted to on-design cases, making 2D simulations sufficient for the purpose of the present investigation. It should be noted that the flow is also modelled as symmetrical with respect to the ejector centerline, which allows the simulation to be performed for only half of the ejector.

The mesh used for the present numerical simulations has been generated via GMSH (Geuzaine and Remacle (2009)). It is primarily comprised of rectangular cells yielding a mainly structured grid, apart from the zone extending from the primary nozzle exit up to the first quarter of the mixing duct (see Fig. 4). Even though the cells used in this unstructured part of the mesh are irregular quadrilaterals, they have angles of almost 90 degrees in order to preserve the orthogonal quality of the mesh. In addition, in this region, the refinement is more important and the aspect ratio of the cells is close to unity in order to correctly capture the supersonic structures at the exit of the primary nozzle. The mesh is also refined in the vertical direction in order to ensure that the centre of the cell adjacent to the wall is always at $y^+ \simeq 1$. In the unstructured zone, a structured layer is used close to the wall to conserve the near-wall refinement all along the ejector (see Fig. 4). In the entire domain, changes in cell volume between adjacent cells are kept relatively low. In total, the mesh is composed of approximately 350,000 cells. For all the results referring to the ejector geometry, note that the origin is fixed on the ejector centerline, at the entry of the mixing duct.

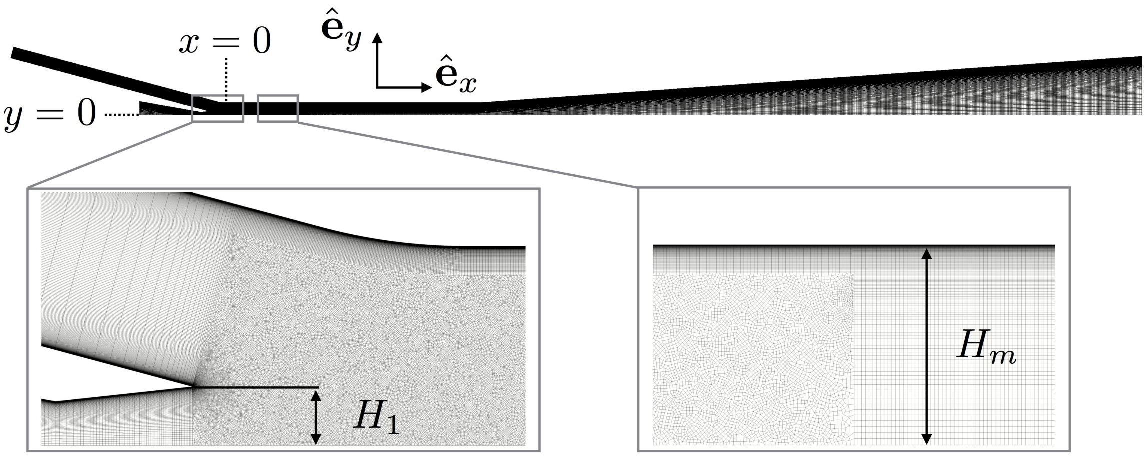

Figure 4: Grid structure of the computational domain for the numerical simulations.

The independence of the numerical results from the computational grid is checked in Fig. 5 by comparing the profile of the Mach number on the axis of the ejector obtained with the mesh described above, referred to as *normal* in Fig. 5, and a *finer* mesh. The latter was obtained by further refining the normal mesh in the axial direction, yielding a grid of approximately 535,000 cells. As may be seen in Fig. 5, the differences between both simulations are negligible. With regard to the entrainment ratio, the relative gap between both calculations is in the order of 0.01%. Hence, the numerical simulations analyzed in this paper have been carried out on the normal mesh which is fully appropriate.

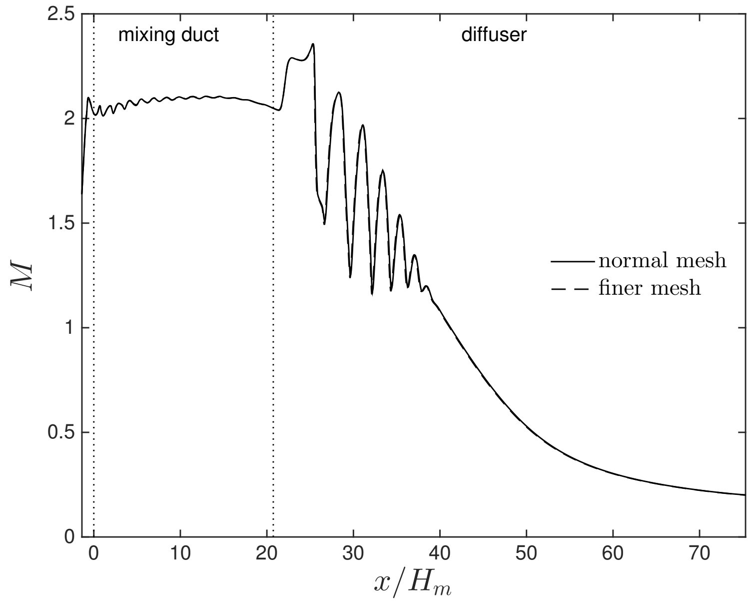

Figure 5: Mach Number profile along the axis of the ejector for grid independence verification - $p_{02}/p_{01} = 0.195$ - $p(x_b)/p_{01} = 0.240$.

2.2.4. Boundary conditions

Walls are all assumed adiabatic. The boundary conditions at both inlets and at the outlet are based on experimental measurements. At both inlets, the pressure and the temperature are specified as stagnation conditions. As mentioned in the introduction, the stagnation conditions of the primary and the secondary streams are indicated with the subscripts 01 and 02, respectively. While the total temperature is approximately the same for both streams and close to the ambient temperature, their stagnation pressures are logically different. In the present study, the selected value of p_{01} is 5.00 [bar], whereas the stagnation pressure of the secondary stream is almost equal to the atmoshperic pressure since it is directly taken from the atmosphere in the experiment. Although small variations of the secondary stagnation pressure were observed in the experiment when changing the back-pressure in the off-design regime (Mazzelli et al. (2015), Lamberts et al. (2018)), all the numerical results presented here have been obtained with the same secondary stagnation pressure, whose value corresponds to the experimental measurement in on-design operation, i.e. $p_{02} = 0.974$ [bar]. This assumption has little effect on the results (Mazzelli et al. (2015)) and allows to highlight the sole impact of the back-pressure on the choking process.

At both inlets, the value of the turbulence intensity (5%) and a specific mixing length are imposed as boundary conditions for the turbulent quantities k and ω, respectively. For more information regarding these conditions, the reader is referred to Lamberts et al. (2017).

As the flow is subsonic at the outlet, the sole variable that is specified is the static pressure, $p(x_b)$. It should be noted that this boundary condition is actually the only difference between all the numerical simulations presented in Section 3.1. The boundary conditions of the different cases are summarized in Table 1.

Case	p_{01} [bar]	p_{02} [bar]	$p(x_b)$ [bar]
A	5.00	0.974	1.20
B			1.60
C			1.70
D			1.80
E			1.85
F			1.90
G			1.95
H			2.00

Table 1: Boundary conditions used in the numerical simulations.

2.2.5. Verification and validation of the numerical method

It is common to validate the CFD model on the basis of one or several characteristic curves (Sriveerakul et al. (2007a), Mazzelli et al. (2015), Croquer et al. (2016a)). Here, the numerical results are validated with experimental data reported in Mazzelli et al. (2015) and the comparison is shown in Fig. 6. As observed in this figure, the entrainment ratio predicted by CFD seems to be in fairly good agreement with experimental data in the on-design regime. Nevertheless, the value of the critical back pressure seems to be overestimated by the numerical simulations, thereby resulting in some discrepancies in off-design conditions. As mentioned in Section 2.2.3, 3D simulations yield better agreement with the experimental data in the off-design regime (Mazzelli et al. (2015)).

For the ejector geometry and reservoir conditions considered here, the entrainment ratio predicted by the compound-choking theory for on-design operation (with the method described in Section 2.1.4) is 52.81%. Actually, it is almost equal to the value obtained with the CFD model (53.07%). This provides a first argument supporting the suitability of the compound-choking theory to model the choking process at play here.

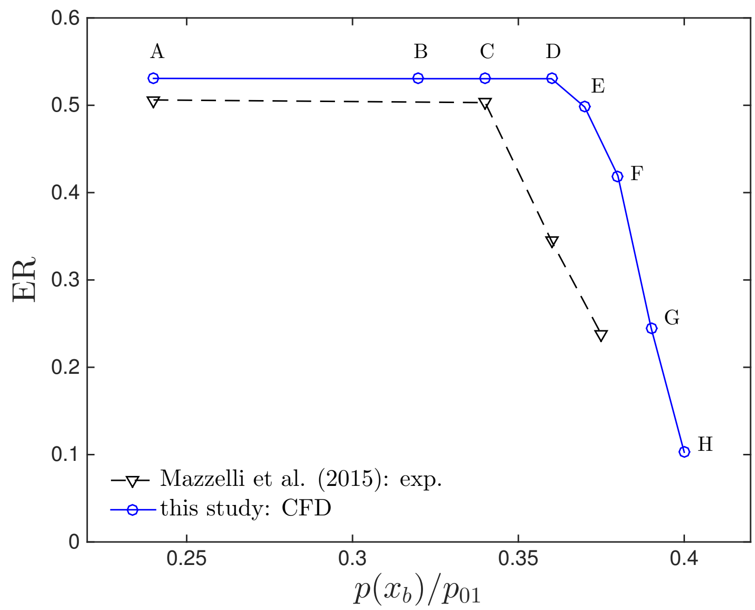

Figure 6: Comparison of the experimental characteristic curve of the ejector with numerical results - $p_{02}/p_{01} = 0.195$.

As the focus is put on local flow phenomena, the numerical results are also validated with experimental data at the local scale. More precisely, the shock reflection pattern at the exit of the primary nozzle has been visualized through schlieren techniques and compared to a numerical pseudo-schlieren. As this study aims at investigating the choking process, the flow structure within the ejector has been validated in the on-design regime (case A in Fig. 6), in which case the flow is relatively stable. The validation in the off-design regime is less straightforward because of flow instabilities and is beyond the scope of the present paper.

Figure 7 shows the comparison between the experimental schlieren image and the numerical pseudo-schlieren, which was generated by computing the vertical gradient of the density field to be consistent with the horizontal orientation of the knife-edge in the experiment. Note that a no-flow picture has been substracted from the raw image obtained in the presence of the flow in order to reduce the impact of the inhomogeneities in the plexiglas. As shown in Fig. 7, the agreement between the numerical results and the experimental schlieren image is very good, thereby giving more credit to the numerical simulations for capturing local flow phenomena. For the present ejector geometry and operating conditions, the expansion waves emanating from the lip of the primary nozzle in Fig. 7 indicate that the motive flow is underexpanded at the nozzle exit plane.

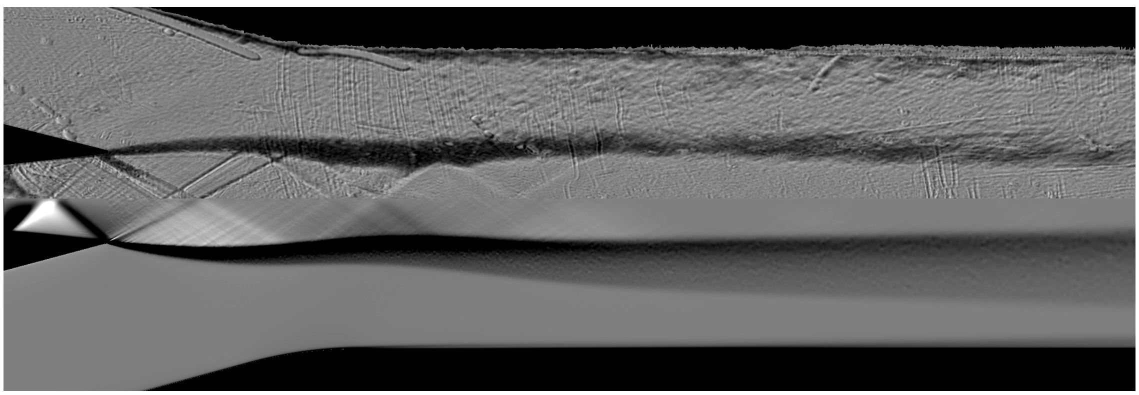

Figure 7: Vertical gradient of the density field: comparison of the experimental (top half) and the numerical (bottom half) schlieren images - $p(x_b)/p_{01} = 0.240$ (case A).

3. Results and discussion

3.1. Numerical evidence of the compound-choking

3.1.1. Sonic line and dividing streamline

In order to highlight the choking process, the analysis of the numerical results is based on the method proposed in Lamberts et al. (2018). It essentially consists in bringing out the region of the ejector where the secondary stream reaches sonic velocities by constructing two fundamental lines in the ejector: the *sonic line* and the *dividing streamline*. The interpretation of both lines is shown in Fig. 8. The sonic line, defined as the iso-contour of Mach number unity, allows to make a distinction between the subsonic and the supersonic regions of the flow (Bartosiewicz et al. (2005), Hemidi et al. (2009b)), whereas the dividing streamline aims at separating the primary and the secondary streams. This line is defined in Lamberts et al. (2017)

as the streamline constructed from the velocity vector field and passing through the point located just above the tip of the primary nozzle. For 2D flows, this streamline actually represents the surface of a stream tube surrounding the primary stream. Since, by construction, there is no average mass flux passing through the surface of a stream tube, the dividing streamline may be interpreted as a virtual separation between the primary and the secondary streams all along the ejector (Lamberts et al. (2017)).

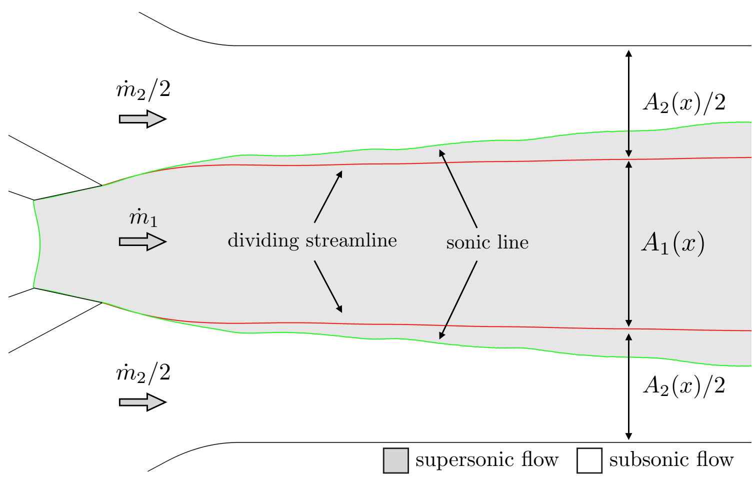

Figure 8: Interpretation of the sonic line and the dividing streamline.

Figure 9 shows the sonic line and the dividing streamline for different values of the back-pressure. The reader is reminded that all these results have been performed with the same reservoir conditions (cfr. Section 2.2.4). For improved readability, the ejector is depicted with a twofold stretching in the vertical direction in Fig. 9. As may be observed in this figure, for on-design operating conditions, there is no sudden transition from subsonic to supersonic velocities in the the secondary stream as the sonic line does not abruptly penetrate it. For cases A and B, the sonic line progressively deviates from the dividing streamline starting from the exit of the primary nozzle and gets very close to the wall near the entry of the diffuser. Hence, for these cases, the secondary stream gradually reaches supersonic velocities by being accelerated through the shear layer. For case E, the ejector operates in the off-design regime and the main portion of the secondary stream logically does not reach supersonic velocities (see Fig. 9(e)).

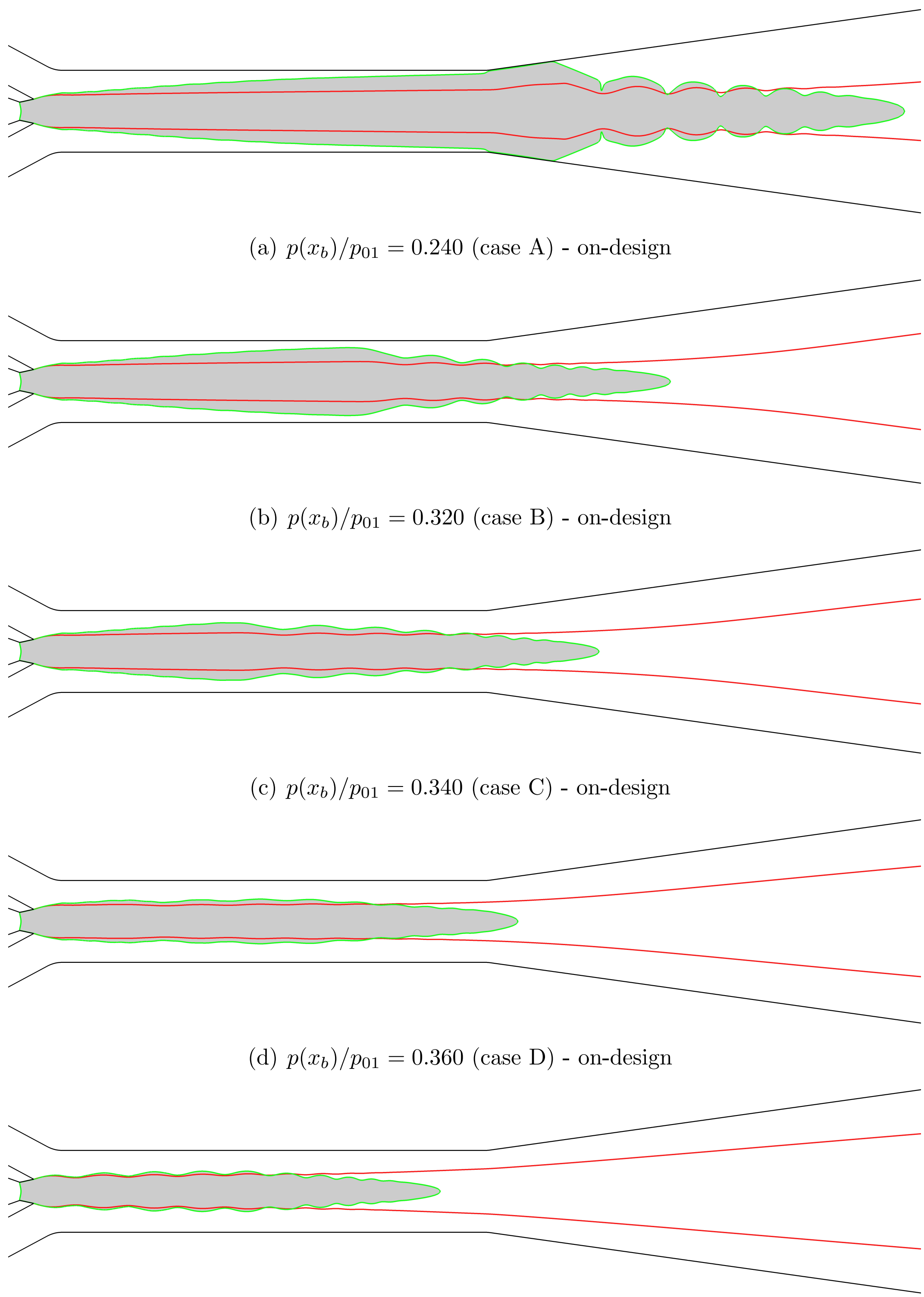

(a) $p(x_b)/p_{01} = 0.240$ (case A) - on-design

(b) $p(x_b)/p_{01} = 0.320$ (case B) - on-design

(c) $p(x_b)/p_{01} = 0.340$ (case C) - on-design

(d) $p(x_b)/p_{01} = 0.360$ (case D) - on-design

(e) $p(x_b)/p_{01} = 0.370$ (case E) - off-design

Figure 9: Sonic line (in green) and dividing streamline (in red) in the ejector for different values of the back pressure. The supersonic region is coloured in grey. The reservoir conditions are reported in Section 2.2.4.

More interestingly, for cases C and D, a significant part of the secondary stream remains subsonic within the entire ejector, even though these operating conditions lie in the on-design regime as indicated by the characteristic curve shown in Fig. 6. The following analysis will give more insights into the choking process at play.

3.1.2. Wall static pressure

The profile of the static pressure at the wall between the nozzle exit plane and the end of the mixing duct is shown in Fig. 10, for the five values of the back-pressure considered above. The significant drop in the static pressure between the nozzle exit and the entry of the mixing duct reflects the contraction and the related acceleration of the secondary stream due to the expansion of the primary stream. Nevertheless, apart from case A, the static pressure does not fall low enough for the secondary stream to reach sonic velocities, at least through an isentropic process. Indeed, the static pressure corresponding to sonic conditions in a 1D isentropic nozzle flow, generally named the critical pressure and noted p^* (to not be confused with the critical back-pressure), is simply given by imposing $M_2 = 1$ in Eq. (6), which yields

$$\frac{p^*}{p_{02}} = \left(1 + \frac{(\gamma - 1)}{2}\right)^{-\frac{\gamma}{(\gamma-1)}} . \tag{8}$$

This expression takes a value close to 0.528 for $\gamma = 1.4$ and is highlighted by a dashed horizontal line in Fig. 10. In contrast, for all the on-design cases, the pressure drop experienced by the secondary stream is consistent with the compound-choking theory as $\overline{p}_{\mathrm{wall}}$ reaches the theoretical value corresponding to the compound-sonic regime, i.e. p^*_{eq} calculated through the procedure described in Section 2.1.4 (see the dash-dotted horizontal line in Fig. 10).

It clearly appears in Fig. 10 that the flow in the ejector is identical up to a certain axial location for the four on-design configurations (cases A-D), although not easily detected in Fig. 9. Indeed, the four curves corresponding to the cases A-D are actually superimposed upstream of the mixing duct entry, and start deviating from each other at different positions downstream in the mixing duct. This is consistent with the fact that the flow is choked for these cases. For case D, which corresponds to a back-pressure near the critical value, the pressure profile starts deviating from the three other curves shortly after the entry of the mixing duct. Results shown in Fig. 10 thus imply that the choking process, i.e. the blockage of the secondary mass flow rate, takes place in the vicinity of the entry of the mixing duct, where the secondary stream is almost entirely subsonic (see Fig. 9 (a) to (d)). Hence, in the present situation, the sonic line is not a good criterion to assess if the flow is choked within the ejector.

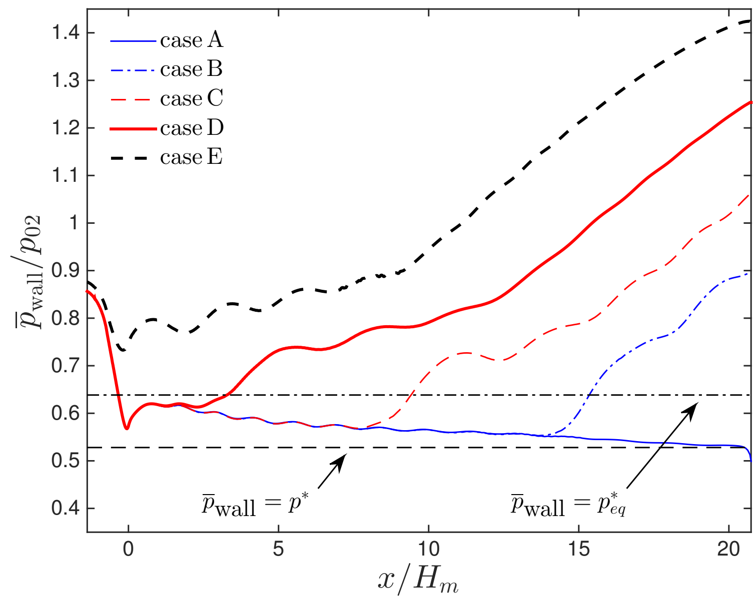

Figure 10: Static pressure profile for different values of the back-pressure (the mixing duct extends from $x/H_m = 0$ to $x/H_m \simeq 20.75$).

These observations are consistent with the compound-choking theory which states that the flow may be choked with a subsonic secondary stream if the primary stream is supersonic. To further confirm that the choking phenomenology is well described by this theory, an equivalent Mach number is calculated all along the ejector by post-processing the numerical results in the next section.

3.1.3. Equivalent Mach number

The equivalent Mach number is obtained through Eq. (2) by post-processing the numerical results. For the calculation of $\beta(x)$, Eq. (1) is used, where the local Mach number of the ith stream is computed according to the definition of Lamberts et al. (2018)

$$M_i(x) = \frac{U_i(x)}{\sqrt{\gamma R T_i(x)}} \qquad (i = 1,\, 2), \tag{9}$$

with $U_i(x)$ a mean velocity

$$U_i(x) = \frac{\dot{m}_i}{\displaystyle\iint_{A_i(x)} \overline{\rho}\, ds} \qquad (i = 1,\, 2), \tag{10}$$

and $T_i(x)$ a mean temperature

$$T_i(x) = \frac{1}{A_i(x)} \iint_{A_i(x)} \hat{T}\, ds \qquad (i = 1,\, 2). \tag{11}$$

In these equations, $A_i(x)$ represents the cross-section of the ith stream, delimited by the dividing streamline (see Fig. 8).

The profile of $M_{eq}(x)$ is shown in Fig. 11 for the five cases considered above, from the exit of the primary nozzle to the entry of the diffuser. For all the on-design cases (cases A-D), the equivalent Mach number reaches unity. In addition, the first location where $M_{eq} = 1$ consistently lies close to the entry of the mixing duct, in the region of the flow that is common to the four cases. In contrast, the equivalent Mach number remains lower than one for the case E which is off-design. Hence, the profiles of the equivalent Mach number are consistent with the compound-choking theory.

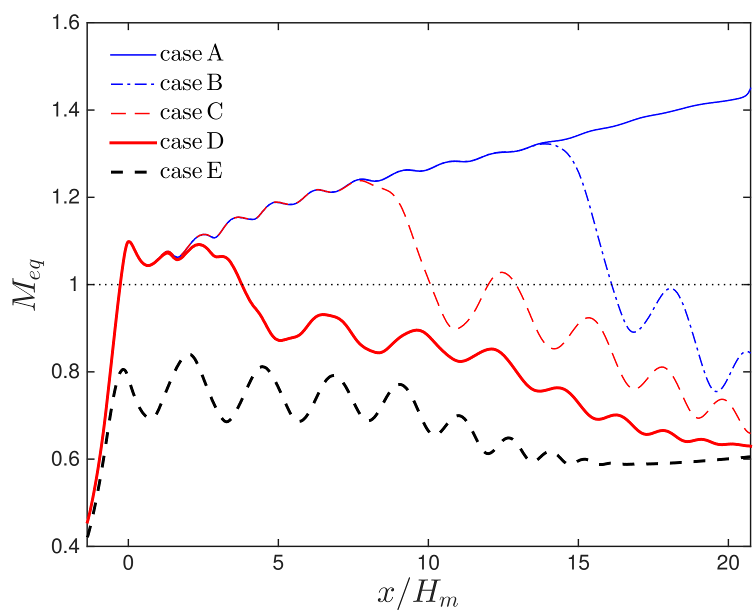

Figure 11: Equivalent Mach number obtained in the post-processing phase of the CFD calculations for different values of the back-pressure (the mixing duct extends from $x/H_m = 0$ to $x/H_m \simeq 20.75$).

Note that the position where the equivalent Mach number reaches unity for on-design cases corresponds to $x/H_m \simeq -0.26$. It is thus not exactly located at the geometrical throat of the ejector but rather a small distance upstream of the mixing duct entry. Yet the total flow area at $x/H_m \simeq -0.26$ is very close to the mixing duct cross-section. The fact that $M_{eq} = 1$ before the entry of the mixing duct is probably due to non-isentropic effects which are not taken into account in the compound-choking theory, as well as the assumption of a uniform pressure profile.

For the present ejector geometry and operating conditions, the phenomenology of the choking thus closely corresponds to the compound-choking theory of Bernstein et al. (1967). However, the Fabri-choking has been evidenced in Lamberts et al. (2018) for the same ejector geometry but with other reservoirs conditions. At this stage, it would be premature to provide explanations on what causes each choking phenomenology to occur. As mentioned in the introduction, a sonic line pattern similar to the one obtained here for case A may be found in numerous numerical studies (Hemidi et al. (2009b), Ji et al. (2010), Ruangtrakoon et al. (2013), Mazzelli and Milazzo (2015), Croquer et al. (2016b), Croquer et al. (2016c)). This would suggest that the compound-choking is more representative of the choking phenomenology in common supersonic ejectors. The following analysis will bring a second argument in favour of the compound-choking as the prevailing choking process in supersonic ejectors.

3.2. Comparison of the compound-choking theory with the experimental data of Huang et al. (1999)

3.2.1. Prediction of the entrainment ratio for various ejector configurations

The experimental data of Huang et al. (1999) using R-141b as refrigerant often serve for the validation of simplified models (Zhu et al. (2007), del Valle et al. (2012), Chen et al. (2017)). Huang et al. (1999) tested 11 axisymmetric ejectors by combining two distinct primary nozzles with 8 different secondary nozzles. The schematic diagram of the geometrical configuration of the different ejectors used in their experimental investigations is shown in Fig. 12. The two primary nozzles differed from each other with regard to their throat and exit diameters (d_t and d_1, respectively), whereas the geometrical differences between the secondary nozzles lay in the diameter of the constant-area region and the inlet converging angle (d_m and θ, respectively). It should be noted that the distance between the nozzle exit plane and the entry of the mixing duct, noted NXP in Fig. 12, was adjusted by Huang et al. (1999) at each operating condition to obtain the best ejector performance. In what follows, in line with Huang et al. (1999), the ejector geometry is characterized by two capital letters, referring to the primary nozzle (A or E) and the secondary nozzle (A to H), respectively. The interested reader is referred to the original article for more information regarding the geometry of the different ejectors.

The reservoir conditions were also varied in the experiment of Huang et al. (1999):

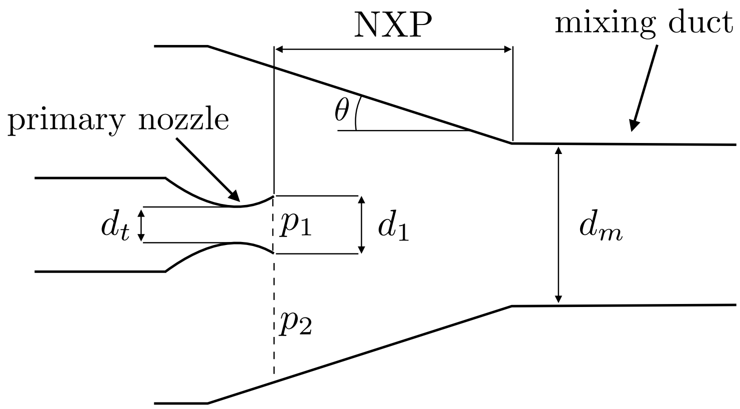

Figure 12: Schematic diagram of the geometrical configuration of the different ejectors used in the experimental investigations of Huang et al. (1999).

the primary stagnation pressure was set to four different values, ranging from 4 to 6.04 [bar], combined with two distinct secondary stagnation pressures (0.4 and 0.47 [bar]). At both inlets, the stagnation temperature corresponded to the saturated temperature of the respective stagnation pressure since the refrigerant was in a saturated vapor state.

In total, Huang et al. (1999) reported 39 different configurations, specifying for each case the on-design entrainment ratio as well as the critical back-pressure (by means of the corresponding saturated vapor temperature). In their experimental investigations, the entrainment ratio ranged from 18.59% to 74.12% while the critical back-pressure varied between 0.75 and 1.5 [bar]. In the present study, only the information regarding the entrainment ratio is used in order to assess the ability of the compound-choking theory to predict the entrainment ratio in on-design conditions, according to the method described in Section 2.1.4. As a reminder, the inputs of the procedure simply consist in the four dimensionless quantities A_m/A_t, p_{02}/p_{01}, T_{02}/T_{01} and γ. The specific heat ratio of R-141b is taken as $\gamma = 1.135$, in accordance with Zhu et al. (2007) who used this value to test their model on the experimental data of Huang et al. (1999).

The prediction of the entrainment ratio with the compound-choking theory is reported in Table 2 (p. 25) for the 39 cases of Huang et al. (1999) and compared to the experimental results. As may be noted from Table 2, the maximum relative deviation of the model with respect to the experimental data regarding the entrainment ratio is less than 15%. In addition, considering the 39 cases, the arithmetic mean of the relative error is positive and close to 4%, implying that the compound-choking theory tends to slightly overestimate the entrainment ratio. This may be partially due to real gas effects which are neglected by the model as the compound-choking theory is currently limited to ideal gas. Accounting for real gas effects when the working fluid is R141b generally tends to lower the predicted entrainment ratio (del Valle et al. (2012)) and could thus further enhance the performance of the compound-choking theory.

To ease the comparison between the model and the experiment, the entrainment ratio predicted by the compound-choking theory is plotted against the experimental data in Fig. 13. As can be seen, most predictions are in the ±10% range when compared to the experimental data.

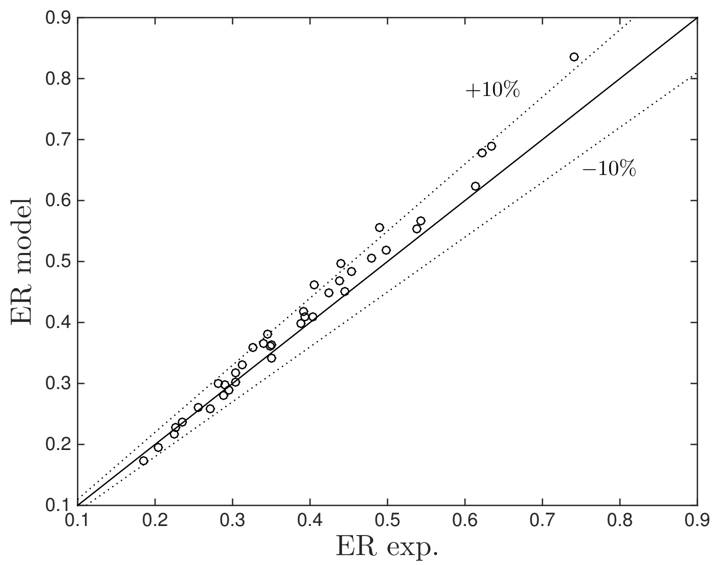

Figure 13: Comparison of the compound-choking theory with the experimental data of Huang et al. (1999).

3.2.2. Comparison with state-of-the-art simplified models

The good performances of the compound-choking theory for the prediction of the entrainment ratio in on-design conditions may be further assessed through a comparison with state-of-the-art 1D models based on the Fabri-choking assumption. In order to make the comparison possible, four models validated against the experimental data of Huang et al. (1999) have been considered here: Huang et al. (1999), Zhu et al. (2007), del Valle et al. (2012) and Chen et al. (2017). Note that these models are more sophisticated than the procedure considered here. More precisely, the model of del Valle et al. (2012) uses a perturbation procedure of linearized and

Case	Ejector	A_m/A_t	p_{01} [bar] ($T_{\mathbf{sat}}$[°C])	p_{02} [bar] ($T_{\mathbf{sat}}$ [°C])	ER (exp)	ER (model)	Error [%]
1	EH	10.64	6.04 (95)	0.4 (8)	0.4377	0.4691	7.16
2	EF	9.83	6.04 (95)	0.4 (8)	0.3937	0.4103	4.21
3	AD	9.41	6.04 (95)	0.4 (8)	0.3457	0.3800	9.92
4	EE	9.17	6.04 (95)	0.4 (8)	0.3505	0.3628	3.50
5	AC	8.28	6.04 (95)	0.4 (8)	0.2814	0.2994	6.38
6	ED	8.25	6.04 (95)	0.4 (8)	0.2902	0.2972	2.43
7	EC	7.26	6.04 (95)	0.4 (8)	0.2273	0.2280	0.32
8	AG	7.73	6.04 (95)	0.4 (8)	0.2552	0.2607	2.15
9	EG	6.77	6.04 (95)	0.4 (8)	0.2043	0.1945	-4.80
10	AA	6.44	6.04 (95)	0.4 (8)	0.1859	0.1722	-7.35
11	AD	9.41	5.38 (90)	0.4 (8)	0.4446	0.4513	1.50
12	AC	8.28	5.38 (90)	0.4 (8)	0.3488	0.3604	3.32
13	AG	7.73	5.38 (90)	0.4 (8)	0.3040	0.3166	4.16
14	AB	6.99	5.38 (90)	0.4 (8)	0.2718	0.2586	-4.86
15	AA	6.44	5.38 (90)	0.4 (8)	0.2246	0.2162	-3.76
16	AD	9.41	4.65 (84)	0.4 (8)	0.5387	0.5545	2.93
17	AC	8.28	4.65 (84)	0.4 (8)	0.4241	0.4491	5.88
18	AG	7.73	4.65 (84)	0.4 (8)	0.3883	0.3982	2.55
19	AB	6.99	4.65 (84)	0.4 (8)	0.3117	0.3305	6.02
20	AA	6.44	4.65 (84)	0.4 (8)	0.2880	0.2808	-2.52
21	AD	9.41	4.00 (78)	0.4 (8)	0.6227	0.6788	9.01
22	AC	8.28	4.00 (78)	0.4 (8)	0.4889	0.5562	13.77
23	AG	7.73	4.00 (78)	0.4 (8)	0.4393	0.4970	13.13
24	AB	6.99	4.00 (78)	0.4 (8)	0.3922	0.4179	6.54
25	AA	6.44	4.00 (78)	0.4 (8)	0.3257	0.3596	10.42
26	EF	9.83	6.04 (95)	0.47 (12)	0.4989	0.5187	3.98
27	EE	9.17	6.04 (95)	0.47 (12)	0.4048	0.4626	14.28
28	AD	9.41	6.04 (95)	0.47 (12)	0.4541	0.4830	6.36
29	AG	7.73	6.04 (95)	0.47 (12)	0.3503	0.3416	-2.50
30	EC	7.26	6.04 (95)	0.47 (12)	0.3040	0.3026	-0.45
31	AA	6.44	6.04 (95)	0.47 (12)	0.2350	0.2357	0.32
32	AD	9.41	5.38 (90)	0.47 (12)	0.5422	0.5676	4.68
33	AG	7.73	5.38 (90)	0.47 (12)	0.4034	0.4085	1.26
34	AA	6.44	5.38 (90)	0.47 (12)	0.2946	0.2889	-1.95
35	AD	9.41	4.65 (84)	0.47 (12)	0.6350	0.6898	8.63
36	AG	7.73	4.65 (84)	0.47 (12)	0.4790	0.5056	5.56
37	AA	6.44	4.65 (84)	0.47 (12)	0.3398	0.3665	7.85
38	AD	9.41	4.00 (78)	0.47 (12)	0.7412	0.8366	12.87
39	AG	7.73	4.00 (78)	0.47 (12)	0.6132	0.6228	1.57

Table 2: Prediction of the entrainment ratio with the compound-choking theory for the 39 experimental ejector configurations of Huang et al. (1999). Error=(model-exp)/exp.

axisymmetric supersonic flow to model 2D effects, whereas the models of Huang et al. (1999), Zhu et al. (2007) and Chen et al. (2017) rely on fitting coefficients. Furthermore, real gas effects are taken into account in del Valle et al. (2012) and Chen et al. (2017). The comparison, based on the error distribution of the different models, is shown in Fig. 14.

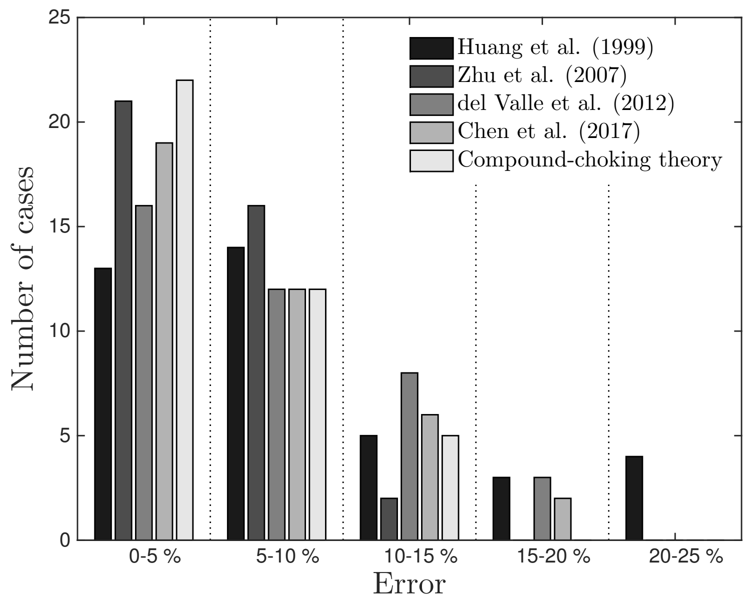

Figure 14: Comparison of the error distribution of the compound-choking theory with state-of-the-art 1D models for the prediction of the entrainment ratio based on the experimental data of Huang et al. (1999).

The model based on the compound-choking theory is found to yield the largest number of cases with errors lower than 5% (22 cases out of 39). Furthermore, with the model of Zhu et al. (2007), the present procedure is the sole whose maximum error is lower than 15%; the other models obtaining errors in the range of 15-20% or more. However, compared to Zhu et al. (2007), the compound-choking theory is based on more robust physical arguments. Indeed, in the model of Zhu et al. (2007), the secondary stream is assumed to reach sonic velocities with a static pressure equal to its inlet pressure, which is not consistent with the fact that the secondary stream is significantly accelerated in the suction chamber. Based on Fig. 14, it may be concluded that the compound choking theory in its simplest form generally performs better than more sophisticated 1D models (based on the Fabri-choking assumption) to predict the entrainment ratio in the on-design regime.

3.2.3. Limitations of the compound-choking theory

The final discussion of this work concerns the limitations of the compound-choking theory for the prediction of the on-design entrainment ratio of supersonic ejectors. Indeed, in certain conditions, the assumptions on which this theory is based (cfr. Section 2.1.1) may be too strong to properly model the flow in the mixing chamber of the ejector, thereby leading to some errors regarding the entrainment ratio. In particular, the compound-choking theory postulates that the flow in each stream is isentropic and one-dimensional. These assumptions may be not quite representative of the flow physics at play between the nozzle exit plane and the choking position in some specific conditions.

As mentioned in Section 2.1.1, the hypothesis of an isentropic process implies that the compound-choking theory neglects the mixing. Of course, in real applications, transfers between the primary and the secondary streams occur through the shear layer, starting from the nozzle exit plane. These transfers probably slightly enhance the entrainment ratio of the ejector. This may cause the compound-choking theory to underestimate the entrainment ratio, in particular when the latter is low. This may be checked in Fig. 15 where the error of the compound-choking theory is shown as a function of the experimental entrainment ratio. As may be observed, all cases in which the theory underestimates the entrainment ratio (i.e. negative error) correspond indeed to relatively low values of the entrainment ratio. The no-mixing assumption is thus the most likely explanation as to why the theoretical prediction of the entrainment ratio may underestimate the experimental value.

Another source of discrepancies between the theory and the experiment may be related to a highly over- or underexpanded primary nozzle. Indeed, if there is a significant mismatch between both streams in terms of static pressure at the nozzle exit plane, large supersonic structures will appear in the core of the primary stream (shock diamonds). In this case, both assumptions of isentropic and one-dimensional flow are not appropriate to model the primary flow, since these shock diamonds are intrinsically 2D and generate irreversibilities.

In order to assess the influence of the expansion level of the primary nozzle on the error made by the compound-choking theory, the ratio between the static pressures of the primary and the secondary streams at the nozzle exit plane, noted respectively p_1 and p_2 in Fig. 12, has been determined with 1D calculations for the 39 cases of Huang et al. (1999). More precisely, Eq. (3) has been used to obtain the static pressure of each stream at the nozzle exit plane from its stagnation conditions, its mass flow rate and its local flow area. The primary mass flow rate has been calculated with Eq. (5) assuming that $A_1^* = A_t$, and the secondary mass flow rate has been subsequently derived from the experimental entrainment ratio. Note that the nozzle

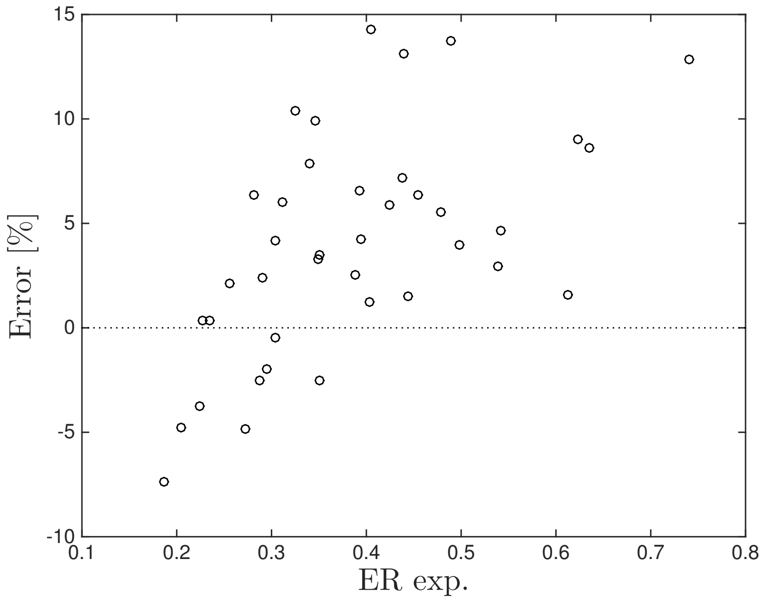

Figure 15: Error of the compound-choking theory as a function of the experimental entrainment ratio based on the experimental data of Huang et al. (1999).

position (noted NXP in Fig. 12) is necessary to determine the cross-sectional area at the nozzle exit plane. Unfortunately, in Huang et al. (1999), the precise value of the NXP is not specified for each case separately. The authors only indicated that its optimal value was found to be around 1.50 d_m, where d_m is the diameter of the constant-area section (see Fig. 12). Hence, the NXP is assumed to be equal to 1.50 d_m in the 1D calculations considered here.

Figure 16 shows the error of the compound-choking theory (regarding the prediction of the entrainment ratio) as a function of p_1/p_2. It consistently appears that the five cases with an error greater than 10 % all have a relatively highly overexpanded nozzle ($p_1/p_2 < 0.85$). In addition, the 22 cases with an error lower than 5 % mainly correspond to a value of p_1/p_2 close to unity (18 cases out of 22 in the range $0.87 < p_1/p_2 < 1.03$). Finally, the error seems to increase when the nozzle is markedly underexpanded, but further experimental investigations are necessary to complete the picture as the maximum value of p_1/p_2 obtained here is around 1.15.

Finally, the compound-choking theory does not take into account the impact of the nozzle exit position (NXP) on the on-design entrainment ratio. Unfortunately, its influence may not be assessed based on the experimental data of Huang et al.

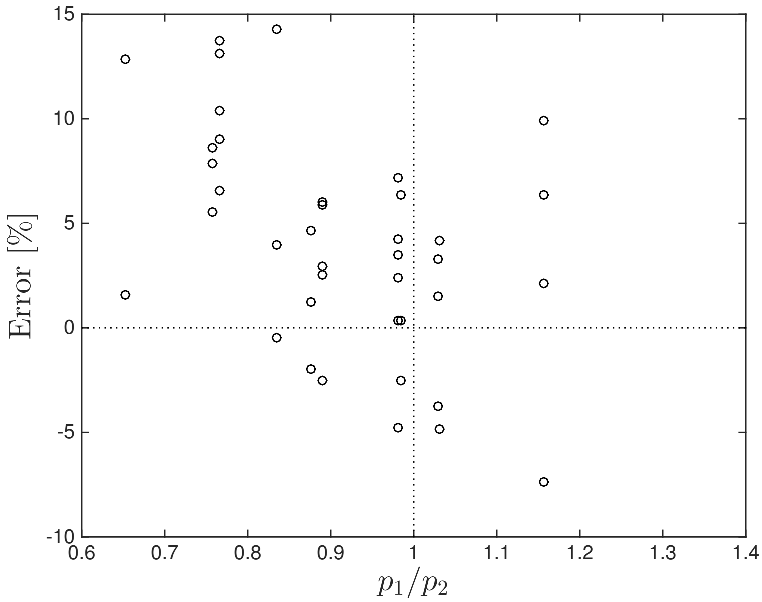

Figure 16: Error of the compound-choking theory as a function of the ratio between the static pressures of the primary and the secondary streams at the nozzle exit plane based on the experimental data of Huang et al. (1999).

(1999) since the ratio NXP/d_m was approximately the same for all the cases. One may expect that the no-mixing hypothesis will gradually lose its validity as this ratio increases. On the other hand, when it is close to zero, the NXP will have a significant impact on the expansion level of the primary nozzle, and thereby on the validity of the assumptions of an isentropic and one-dimensional flow in the primary stream. Ultimately, for an ejector with a geometrical configuration such that the nozzle exit is located in the mixing duct (sometimes referred to as constant-area mixing), the performance of the compound-choking theory is likely to be more limited. Here again, further experimental investigations are necessary.

4. Conclusion

In this paper, an in-depth analysis of the choking process in the post-processing phase of numerical simulations has been performed for the same ejector geometry than Lamberts et al. (2018) but with other reservoir conditions. Here, it was shown that the secondary stream does not reach sonic conditions in a hypothetical throat as postulated in Fabri and Siestrunck (1958). Moreover, a significant part of the secondary stream remains subsonic within the entire ejector for some operating conditions lying in the on-design regime. Actually, for the present ejector geometry and operating conditions, the choking process, i.e. the blockage of the secondary mass flow rate, takes place close to the entry of the mixing duct, at a position that is common to all on-design cases and where the secondary stream is almost entirely subsonic. The observed choking phenomenology was found to be properly described by a theory developed in the 1960's and known as the compound-choking theory, which states that a two-stream compound-compressible nozzle flow may be choked with a subsonic stream if the other one is supersonic, as the combination of the two streams may behave like a sonic stream. The profile of the equivalent Mach number further corroborated the adequacy of the compound-choking theory to yield a physical explanation of the choking phenomenology highlighted with the numerical results. Hence, the sonic line is not always a good criterion to assess if the flow is choked within a supersonic ejector.

In order to determine the choking theory that is more adequate to describe the choking process occurring in supersonic ejectors, the ability of the compound-choking theory to predict the on-design entrainment ratio has been assessed on the experimental data of Huang et al. (1999). This theory has been used in its simplest form according to a methodology proposed by Bernstein et al. (1967), for known reservoir conditions and geometrical parameters. The computational procedure simply consists in simultaneously solving two algebraic equations. Most predictions of the compound-choking theory are in the $\pm 10\%$ range when compared to the experimental data of Huang et al. (1999). Moreover, based on these experimental results, the compound-choking theory is shown to generally perform better than state-of-the-art 1D models relying on the Fabri-choking assumption for the prediction of the on-design entrainment ratio.

This work is the first study providing quantitative arguments based on i) numerical simulations and ii) a comparison to comprehensive experimental results to highlight the suitability of the compound-choking theory for modeling the choking process in most supersonic ejectors. Ultimately, the use of the compound-choking theory could lead to more efficient simplified models of supersonic ejectors.

Acknowledgements

The present work benefited from the computational resources provided by the supercomputing facilities of the Université catholique de Louvain (CISM/UCL) and the Consortium des Équipements de Calcul Intensif en Fédération Wallonie Bruxelles (CÉCI) funded by the Fond de la Recherche Scientifique de Belgique (F.R.S.-FNRS) under Convention No. 2.5020.11.

References

Addy, A., Dutton, J., Mikkelsen, C., Mikkelsen, C., of MECHANICAL, I. U. A. U. D., ENGINEERING., I., 1981. Supersonic Ejector-Diffuser Theory and Experiments. Defense Technical Information Center.
URL https://books.google.be/books?id=Jl0KGwAACAAJ

Ameur, K., Aidoun, Z., Ouzzane, M., 2016. Modeling and numerical approach for the design and operation of two-phase ejectors. Applied Thermal Engineering 109, 809 – 818.
URL http://www.sciencedirect.com/science/article/pii/S1359431114010205

Bartosiewicz, Y., Aidoun, Z., Desevaux, P., Mercadier, Y., 2003. Cfd-experiments integration in the evaluation of six turbulence models for supersonic ejectors modeling.

Bartosiewicz, Y., Aidoun, Z., Desevaux, P., Mercadier, Y., 2005. Numerical and experimental investigations on supersonic ejectors. International Journal of Heat and Fluid Flow 26 (1), 56 – 70.
URL http://www.sciencedirect.com/science/article/pii/S0142727X04001158

Bernstein, A., Heiser, W. H., Hevenor, C., 09 1967. Compound-compressible nozzle flow. Journal of Applied Mechanics 34 (3), 548–554.
URL http://dx.doi.org/10.1115/1.3607742

Besagni, G., Inzoli, F., 2017. Computational fluid-dynamics modeling of supersonic ejectors: Screening of turbulence modeling approaches. Applied Thermal Engineering 117, 122 – 144.
URL http://www.sciencedirect.com/science/article/pii/S1359431116328290

Besagni, G., Mereu, R., Inzoli, F., 2016. Ejector refrigeration: A comprehensive review. Renewable and Sustainable Energy Reviews 53, 373 – 407.
URL http://www.sciencedirect.com/science/article/pii/S1364032115009223

Chen, W., Liu, M., Chong, D., Yan, J., Little, A. B., Bartosiewicz, Y., 2013. A 1d model to predict ejector performance at critical and sub-critical operational regimes. International Journal of Refrigeration 36 (6), 1750 – 1761.
URL http://www.sciencedirect.com/science/article/pii/S0140700713000984

Chen, W., Shi, C., Zhang, S., Chen, H., Chong, D., Yan, J., 2017. Theoretical analysis of ejector refrigeration system performance under overall modes. Applied

Energy 185, 2074 – 2084, clean, Efficient and Affordable Energy for a Sustainable Future.
URL http://www.sciencedirect.com/science/article/pii/S0306261916300915

Chou, S., Yang, P., Yap, C., 2001. Maximum mass flow ratio due to secondary flow choking in an ejector refrigeration system. International Journal of Refrigeration 24 (6), 486 – 499.
URL http://www.sciencedirect.com/science/article/pii/S0140700700000748

Chunnanond, K., Aphornratana, S., 2004a. Ejectors: applications in refrigeration technology. Renewable and Sustainable Energy Reviews 8 (2), 129–155.
URL http://EconPapers.repec.org/RePEc:eee:rensus:v:8:y:2004:i:2:p:129-155

Chunnanond, K., Aphornratana, S., 2004b. An experimental investigation of a steam ejector refrigerator: the analysis of the pressure profile along the ejector. Applied Thermal Engineering 24 (23), 311 – 322.
URL http://www.sciencedirect.com/science/article/pii/S1359431103002539

Croquer, S., Poncet, S., Aidoun, Z., 2016a. Turbulence modeling of a single-phase r134a supersonic ejector. part 1: Numerical benchmark. International Journal of Refrigeration 61, 140 – 152.
URL http://www.sciencedirect.com/science/article/pii/S0140700715002376

Croquer, S., Poncet, S., Aidoun, Z., 2016b. Turbulence modeling of a single-phase R134a supersonic ejector. part 2: Local flow structure and exergy analysis. International Journal of Refrigeration 61, 153 – 165.
URL http://www.sciencedirect.com/science/article/pii/S0140700715002364

Croquer, S., Poncet, S., Galanis, N., 2016c. Comparison of ejector predicted performance by thermodynamic and cfd models. International Journal of Refrigeration 68, 28 – 36.
URL http://www.sciencedirect.com/science/article/pii/S0140700716300809

del Valle, J. G., Jabardo, J. M. S., Ruiz, F. C., Alonso, J. S. J., 2012. A one dimensional model for the determination of an ejector entrainment ratio. International Journal of Refrigeration 35 (4), 772 – 784.
URL http://www.sciencedirect.com/science/article/pii/S0140700711003008

del Valle, J. G., Sierra-Pallares, J., Carrascal, P. G., Ruiz, F. C., 2015. An experimental and computational study of the flow pattern in a refrigerant ejector. validation of turbulence models and real-gas effects. Applied Thermal Engineering

89, 795 – 811.
URL http://www.sciencedirect.com/science/article/pii/S1359431115006237

Fabri, J., Siestrunck, R., 1958. Supersonic air ejectors. Advances in Applied Mechanics 5, 1–34.

Galanis, N., Sorin, M., 2016. Ejector design and performance prediction. International Journal of Thermal Sciences 104, 315 – 329.
URL http://www.sciencedirect.com/science/article/pii/S1290072916000351

Geuzaine, C., Remacle, J.-F., 2009. Gmsh: A 3-D finite element mesh generator with built-in pre-and post-processing facilities. International Journal for Numerical Methods in Engineering 79 (11), 1309–1331.

Greenshields, C. J., Weller, H. G., Gasparini, L., Reese, J. M., 2010. Implementation of semi-discrete, non-staggered central schemes in a colocated, polyhedral, finite volume framework, for high-speed viscous flows. International Journal for Numerical Methods in Fluids 63, 1–21.

He, S., Li, Y., Wang, R., 2009. Progress of mathematical modeling on ejectors. Renewable and Sustainable Energy Reviews 13 (8), 1760 – 1780.
URL http://www.sciencedirect.com/science/article/pii/S1364032108001779

Hedges, K. R., Hill, P. G., 09 1974. Compressible flow ejectors: Part ii—flow field measurements and analysis. Journal of Fluids Engineering 96 (3), 282–288.
URL http://dx.doi.org/10.1115/1.3447153

Hemidi, A., Henry, F., Leclaire, S., Seynhaeve, J.-M., Bartosiewicz, Y., 2009a. CFD analysis of a supersonic air ejector. part I: Experimental validation of single-phase and two-phase operation. Applied Thermal Engineering 29 (89), 1523 – 1531.
URL http://www.sciencedirect.com/science/article/pii/S1359431108003037

Hemidi, A., Henry, F., Leclaire, S., Seynhaeve, J.-M., Bartosiewicz, Y., 2009b. CFD analysis of a supersonic air ejector. part II: Relation between global operation and local flow features. Applied Thermal Engineering 29 (1415), 2990 – 2998.
URL http://www.sciencedirect.com/science/article/pii/S1359431109000969

Hoge, H. J., Segars, R. A., 2017/12/14 1965. Choked flow - a generalization of the concept and some experimental data. AIAA Journal 3 (12), 2177–2183.
URL https://doi.org/10.2514/3.3343

Huang, B., Chang, J., Wang, C., Petrenko, V., 1999. A 1-D analysis of ejector performance. International Journal of Refrigeration 22 (5), 354 – 364.
URL http://www.sciencedirect.com/science/article/pii/S0140700799000043

Ji, M., Utomo, T., Woo, J., Lee, Y., Jeong, H., Chung, H., 2010. CFD investigation on the flow structure inside thermo vapor compressor. Energy 35 (6), 2694 – 2702.
URL http://www.sciencedirect.com/science/article/pii/S0360544209005222

Kong, F., Kim, H., 2015. Analytical and computational studies on the performance of a two-stage ejectordiffuser system. International Journal of Heat and Mass Transfer 85, 71 – 87.
URL http://www.sciencedirect.com/science/article/pii/S0017931015001350

Kurganov, A., Noelle, S., Petrova, G., Mar. 2001. Semidiscrete central-upwind schemes for hyperbolic conservation laws and hamilton–jacobi equations. SIAM J. Sci. Comput. 23 (3), 707–740.
URL http://dx.doi.org/10.1137/S1064827500373413

Kurtz, Jr., E. F., 05 1976. Theoretical model for predicting steam-ejector performance. Journal of Engineering for Industry 98 (2), 645–651.
URL http://dx.doi.org/10.1115/1.3438962

Lamberts, O., Chatelain, P., Bartosiewicz, Y., 2017. New methods for analyzing transport phenomena in supersonic ejectors. International Journal of Heat and Fluid Flow 64, 23 – 40.
URL http://www.sciencedirect.com/science/article/pii/S0142727X16304222

Lamberts, O., Chatelain, P., Bartosiewicz, Y., 2018. Numerical and experimental evidence of the fabri-choking in a supersonic ejector. International Journal of Heat and Fluid Flow 69, 194 – 209.
URL https://www.sciencedirect.com/science/article/pii/S0142727X1730752X

Lear, W. E., Sherif, S. A., Parker, G. M., 2000. Effect of fabri choking on the performance of two-phase jet pumps. In: Collection of Technical Papers. 35th Intersociety Energy Conversion Engineering Conference and Exhibit (IECEC) (Cat. No.00CH37022). Vol. 2. pp. 1190–1197 vol.2.

Ma, Z., Bao, H., Roskilly, A. P., 2017. Thermodynamic modelling and parameter determination of ejector for ejection refrigeration systems. International Journal of Refrigeration 75, 117 – 128.
URL http://www.sciencedirect.com/science/article/pii/S0140700716304170

Mazzelli, F., Little, A. B., Garimella, S., Bartosiewicz, Y., 2015. Computational and experimental analysis of supersonic air ejector: Turbulence modeling and assessment of 3D effects. International Journal of Heat and Fluid Flow 56, 305 – 316. URL http://www.sciencedirect.com/science/article/pii/S0142727X15001101

Mazzelli, F., Milazzo, A., 2015. Performance analysis of a supersonic ejector cycle working with r245fa. International Journal of Refrigeration 49, 79 – 92. URL http://www.sciencedirect.com/science/article/pii/S014070071400259X

Munday, J. T., Bagster, D. F., 1977. A new ejector theory applied to steam jet refrigeration. Industrial & Engineering Chemistry Process Design and Development 16 (4), 442–449. URL http://dx.doi.org/10.1021/i260064a003

Pearson, H., Holliday, J. B., Smith, S. F., 1958. A theory of the cylindrical ejector supersonic propelling nozzle. The Journal of the Royal Aeronautical Society 62 (574), 746751.

Rao, S. M., Jagadeesh, G., 2014. Observations on the non-mixed length and unsteady shock motion in a two dimensional supersonic ejector. Physics of Fluids 26 (3), 036103.

Ruangtrakoon, N., Thongtip, T., Aphornratana, S., Sriveerakul, T., 2013. CFD simulation on the effect of primary nozzle geometries for a steam ejector in refrigeration cycle. International Journal of Thermal Sciences 63, 133 – 145. URL http://www.sciencedirect.com/science/article/pii/S1290072912002098

Shapiro, A., 1953. The dynamics and thermodynamics of compressible fluid flow. No. vol. 1 in The Dynamics and Thermodynamics of Compressible Fluid Flow. Ronald Press Co. URL https://books.google.co.nz/books?id=OvxQAAAAMAAJ

Sriveerakul, T., Aphornratana, S., Chunnanond, K., 2007a. Performance prediction of steam ejector using computational fluid dynamics: Part 1. validation of the CFD results. International Journal of Thermal Sciences 46 (8), 812 – 822. URL http://www.sciencedirect.com/science/article/pii/S129007290600189X

Sriveerakul, T., Aphornratana, S., Chunnanond, K., 2007b. Performance prediction of steam ejector using computational fluid dynamics: Part 2. flow structure of a steam ejector influenced by operating pressures and geometries. International

Journal of Thermal Sciences 46 (8), 823 – 833.
URL http://www.sciencedirect.com/science/article/pii/S1290072906001876

Varga, S., Oliveira, A. C., Diaconu, B., 2009. Numerical assessment of steam ejector efficiencies using CFD. International Journal of Refrigeration 32 (6), 1203 – 1211.
URL http://www.sciencedirect.com/science/article/pii/S0140700709000073

Weller, H. G., Tabor, G., Jasak, H., Fureby, C., Nov. 1998. A tensorial approach to computational continuum mechanics using object-oriented techniques. Comput. Phys. 12 (6), 620–631.
URL http://dx.doi.org/10.1063/1.168744

Wilcox, D., 2006. Turbulence Modeling for CFD (Third Edition). DCW Industries, Incorporated.

Zegenhagen, M., Ziegler, F., 2015. A one-dimensional model of a jet-ejector in critical double choking operation with R134a as a refrigerant including real gas effects. International Journal of Refrigeration 55, 72 – 84.
URL http://www.sciencedirect.com/science/article/pii/S0140700715000687

Zhu, Y., Cai, W., Wen, C., Li, Y., 2007. Shock circle model for ejector performance evaluation. Energy Conversion and Management 48 (9), 2533 – 2541.
URL http://www.sciencedirect.com/science/article/pii/S0196890407000957

Zucker, R., Biblarz, O., 2002. Fundamentals of Gas Dynamics. Wiley.
URL https://books.google.be/books?id=nc42a_YqvgcC